Journal of Thermal Analysis and Calorimetry, Vol. 90 (2007) 3, 699–706

EFFECT OF CITRATE TO NITRATE RATIO ON THE DECOMPOSITION CHARACTERISTICS AND PHASE FORMATION OF ALUMINA

*S. Banerjee and P. Sujatha Devi**

Electroceramics Division, Central Glass and Ceramic Research Institute, Kolkata 700 032, India

This paper reports the effect of the variation of citrate to nitrate ratio on the thermal decomposition characteristics of alumina precursor and the properties of nanocrystalline alumina synthesized using this auto-ignition process. The technique involves the auto-ignition of a citrate-nitrate gel occurring between $Al(NO_3)_3$ and citric acid to yield an ash powder that upon calcination at 1373 K produced α-alumina. The auto-ignition was restricted to a particular range of citrate to nitrate ratio in the gel. The resulting powder exhibited large surface area (40–50 m^2 gm^{-1}) and fine crystallite size. It was established from various characterization techniques that the alumina powder prepared with a C/N ratio of 0.3 has got the optimum powder characteristics compared to the rest of the batches, thus establishing the importance of maintaining a stoichiometric or near stoichiometric C/N ratio. The process has a higher degree of reproducibility and a good potential for large-scale production of alumina.

Keywords: *alumina, citrate–nitrate process, thermal analysis*

Introduction

Alumina is an advanced ceramic material with unique physical properties which has a wide range of uses in areas such as abrasives, refractories, lasers, high alumina cements, toughened ceramics and substrates for microelectronic computer chips and other electronic packaging. Besides, porous alumina having large surface area, and other unique physical, chemical, thermal, optical and mechanical properties, is being used as catalyst carriers, membranes and humidity sensors. The formation of α-alumina from boehmite, diaspore or γ-alumina occurs through a series of reactions depending on the starting materials. For example, the formation of α-phase from γ-phase occurs via a series of polymorphic transformations such as $\gamma\text{-}Al_2O_3 \rightarrow \delta \rightarrow \theta \rightarrow \alpha\text{-}Al_2O_3$. Boehmite on the other hand, first converts to the metastable γ-alumina at 773 K which then transforms to δ-alumina and θ-alumina, and eventually to the stable α-alumina (corundum) at 1373–1473 K. On heating, all the polymorphic forms of alumina finally transform to the thermodynamically stable α-alumina above 1473 K. Various wet chemical methods are available to prepare reactive alumina at low temperatures [1–10]. For example, Wang *et al.*, [11] reported the synthesis of thermally stable alpha alumina of specific surface area around 20 m^2 gm^{-1} after calcination above 1373 K for 10 h. The ultrasonic spray pyrolysis (USP) technique was used by Kucza *et al.*, [12] for preparing alpha alumina powders. Maruthiprasad *et al.*, [13] on the other hand, have prepared alumina precursors by precipitation from homogeneous solution method. Mekasuwandumrong *et al.*, [14] have used a rather new solvothermal synthesis using aluminium isopropoxide in mineral oil at 523–573 K for 2 h for preparing X-alumina which directly transforms to alpha alumina after calcination at 1473 K. Many reports are there on preparation of alpha alumina using different precursors other than aluminum nitrate. For example, Ibrahim *et al.*, [15] have used aluminum chloride as a precursor where the produced alpha alumina shows 90.9% density after sintering at 1973 K. Sivakumar *et al.*, [16] on the other hand has used combustion chemical vapor deposition technique to synthesize alpha alumina. Among the various wet chemical methods, combustion process has gained considerable attention recently due to its simplicity, reproducibility, and more importantly the lower cost of production, less time and energy consumption. Few reports are available on the combustion synthesis of traditional alumina using aluminum nitrate and fuels such as urea, citric acid and sucrose [17–27]. For example, Hernandez *et al.*, [24] synthesised alpha alumina by a polymeric Pechini process. Toniolo *et al.*, [25] have synthesized alpha alumina powders by glycine-nitrate combustion process where well crystallized alpha alumina of specific surface area around 15 m^2 gm^{-1} was formed after calcination above 1373 K. Li *et al.*, [26–27] have studied the thermal decomposition characteristics of alumina

* Author for correspondence: e-mail: psujathadevi@cgcri.res.in

1388–6150/$20.00

Akadémiai Kiadó, Budapest, Hungary
Springer, Dordrecht, The Netherlands

precursors by a gel combustion route using aluminum nitrate and citric acid as raw materials. Few reports are also there on the study of kinetics of formation and reactions of alpha alumina, aluminium oxides and hydroxides [28–31]. In contrast to the conventional amorphous-citrate precursor process, where the citrate to metal ion ratio was usually fixed at unity [32–34], here, we have varied the citrate to nitrate ratio and studied their effect on the synthesis of nano-size alumina powder. The product obtained from an optimized composition appears to have a higher degree of purity, homogeneity, and better sinterability. The citrate-nitrate auto-ignition process was first developed in our laboratory for the low temperature synthesis of phase pure perovskite and superconducting oxides, but later extended for the synthesis and large-scale production of other multicomponent oxides as well [35–39]. Briefly, in this process, a thermally induced oxidation–reduction reaction between citrate ions and nitrate ions results in a self-propagating controlled exothermic reaction. The main advantage of this process, however, lies in the overall simplicity of the entire course of processing.

Experimental

All the chemicals used were of analytical reagent grade. In this process aqueous solution of 0.2(M) $Al(NO_3)_3 \cdot 9H_2O$ was prepared and appropriate amounts of citric acid was added to it by varying the citrate to nitrate (C/N) ratio from 1.0 down to 0.08. The rest of the synthetic procedure is similar to what has been followed earlier [22]. The resultant pyrophorated dried mass was hand ground in an agate mortar and the powders were calcined at various temperatures (773, 1073 and 1373 K) for 6 h to obtain phase pure powders of alumina. In Table 1, different batches of gels with their preparation conditions are tabulated. The powders calcined at 1073 K were uniaxially pressed and sintered at 1723 and 1823 K and densities of the samples were measured by Archimede's principle.

Characterization of the precursor gel and the powder samples

The thermal decomposition characteristics of the dried gel precursors were studied by means of differential thermal analysis (DTA) and thermogravimetric analysis (TG) techniques. These studies were carried out from room temperature to 1273 K at a heating rate of 10 K min^{-1} in a NETZSCH thermal analyzer unit (409C) using α-alumina as a reference for DTA. The room temperature powder X-ray diffraction (XRD) was carried out both on the combustion synthesized as well as on calcined powders for phase identification and crystallite size estimation and was carried out using a Philips X-ray diffractometer (PW1730) with CuK_α radiation at a 2θ scan rate of 2° min^{-1}. Particle size analysis of the calcined powders was carried out using a Sedigraph 5100 Micromeritics particle size analyzer. Surface area analysis of the calcined powders was carried out on a Micromeritics Gemini II 2370 surface area analyzer. The specific surface area (SSA) was converted into particle size assuming that the particles are closed spheres with smooth surface and uniform size using Eq. (1)

$$D_{BET}=6\cdot10^3/d_{th}S_{BET} \quad (1)$$

where, d_{th} is the theoretical density of the material under consideration, D_{BET} is the average particle size in nm and S_{BET} is the specific surface area expressed in m^2 gm^{-1}. Microstructural studies on the powder samples were carried out on a Leo 430i scanning electron microscope.

Results and discussion

General characteristics

All the gel compositions were white or yellowish white, hygroscopic, and sticky in nature. As the citrate content in the gel increased, the gel samples became more viscous. The color of the uncalcined powder samples on the other hand varied with change in the C/N ratio. The powder samples derived from gels G1 and G2 were white in colour, G3 and G4 were yellow, G5 was deep brown and G6 was black in color.

Table 1 Preparation conditions and decomposition nature of the Al_2O_3 gel precursors

Sample numbers	Sample label	C/N ratio	Characteristic observation of the decomposition	Color of the decomposed ash powder (A)
1	G1	0.08	Fire (no flame)	White
2	G2	0.1	Fire (no flame)	Yellowish white
3	G3	0.3	No fire	Yellow
4	G4	0.5	No fire	Light brown
5	G5	0.7	Slow decomposition	Black
6	G6	1.0	Slow decomposition	Dark brown

TG and DTA studies on gel samples

The thermal behavior of the dried gels was found to depend strongly on the C/N ratio of the starting solution. Figures 1–3 illustrate the simultaneous TG/DTA curves of the representative gel samples. Depending upon the initial C/N ratio, the decomposition behavior of the gels could be classified into three distinct categories.

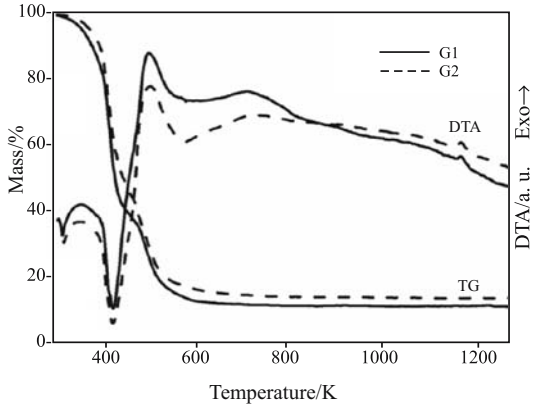

Fig. 1 TG/DTA analysis of the G1 and G2 gel samples

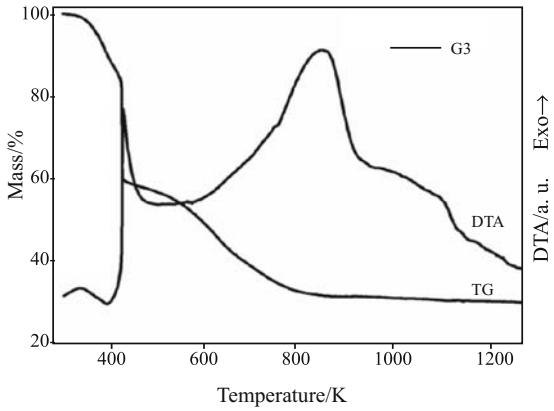

Fig. 2 TG and DTA data of the G3 gel sample prepared with a C/N ratio of 0.3

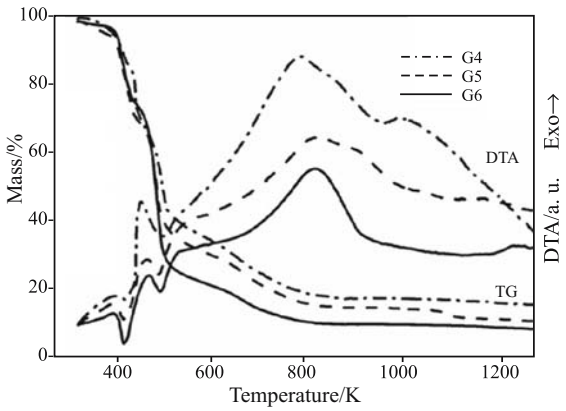

Fig. 3 TG and DTA graphs of the G4, G5 and G6 gel samples with a higher C/N ratios of 0.5, 0.7 and 1 respectively

First category

When the C/N ratio was too low, i.e., 0.08 and 0.1 (G1 and G2) the TG curves showed a total mass loss of more than 85%. The thermal decomposition appears to be a multi-step decomposition reaction (Fig. 1). Another interesting phenomenon is the presence of two endothermic peaks in the DTA. The weak peak around 317–320 K can be attributed primarily due to the dehydration of the gel and the strong endothermic peak around 423 K to its initial thermal decomposition reaction. The endothermic decomposition around 423 K is accompanied by a series of exothermic reactions, corresponding to the decomposition of the citrate complex, oxidation of the intermediate compounds and crystallization of alpha alumina. Here, the major reaction is the endothermic decomposition of the precursor. Beyond 550 K, TG do not indicate any mass loss confirming the completion of major decomposition reaction at this temperature. Interestingly, the DTA curves of G1 and G2 showed weak exothermic peaks around 1159–1160 K, which are ascribed to the transformation of γ to α alumina phase.

Second category

In the case of G3, where a slightly higher C/N ratio of 0.3 was used, the thermal decomposition nature was found to be different (Fig. 2). The major decomposition reaction appeared to be similar to the decomposition of an auto-ignition reaction with a single step reaction with a sharp fall in mass followed by a strong exothermic reaction occurring around 435 K as evident from Fig. 2 [18–21]. As also evident from the DTA curve, the onset of this combustion process starts around 423 K and because of this combustion process, the temperature of the system as a whole increased to 523 K as evident from the DTA peak temperature. The abrupt fall in mass between 423 and 473 K in the TG plot is evidence for a single step decomposition of the gel during the combustion. This in contrast to a multi-step decomposition behavior normally observed for the amorphous citrate gels [16, 17]. This single step decomposition behaviour associated with a very sharp and intense exotherm is a clear indication of an auto-ignited combustion process. As has been reported earlier, this auto-combustion arises due to a highly exothermic anionic oxidation-reduction reaction between the citrate and the nitrate ions releasing a large amount of gases [18–21]. This decomposition reaction is accompanied by a thermally stable plateau at 473 K, which indicates the formation of a stable intermediate product, which further undergoes a slow decomposition within the temperature range of 500–873 K.

Third category

The decomposition characteristics of gels G4, G5 and G6 represent typical multistep decomposition reactions (Fig. 3). It is evident from the TG curve that the mass loss occurs in three steps. The first mass loss at 399 K is accompanied by an endothermic reaction and the second mass loss at 435 K is accompanied by an exothermic reaction. The first reaction is due to the dehydration of bound water to the Al-citrate complex and the second reaction by the decomposition and oxidation of the Al-citrate complex. Moreover, TG also indicates that in addition to the major decomposition reaction, a relatively small second decomposition also occurs at around 473–873 K, which is associated with a very broad exothermic peak. The decomposition of the gel appears to be complete within 873 K. The nature of decomposition of the gel samples is shown in Table 1.

The thermal characteristics associated with the exothermic decomposition of the gel samples are tabulated in Table 2. The calculated enthalpy change, $-\Delta H$, was smallest for the G5 and G6 batches where a higher C/N ratio was used. The enthalpy change is highest for the G3 batch with a C/N ratio of 0.3.

Based on the concept of propellant chemistry, the ratio of the oxidizing valency of the metal nitrates (O) to the reducing valency of the fuel (R) should be unity to get the maximum exothermicity during a combustion reaction. We have calculated the (O/R) ratio of oxidant to fuel for the different batches where the C/N ratio was varied. The oxidizing and reducing valencies were calculated by considering the valencies of elements as +4 for C, +1 for H, –2 for O, and 0 for N and +3 for Al. Thus, the oxidizing valency for $Al(NO_3)_3$ is –15 and the reducing valency for citric acid is +18.

For a complete combustion reaction, the oxidant and the fuel should be present in a stoichiometric ratio. Following Pederson's reaction model, the combustion reaction involving aluminum nitrate and citric acid may be represented as follows:

$$18Al(NO_3)_3+15C_6H_8O_7\rightarrow 90CO_2+27N_2+60H_2O+9Al_2O_3 \quad (2)$$

As per the above equation, the C/N ratio has to be around 0.277 for an idealized situation where the (O/R) ratio is expected to be unity and the enthalpy of the reaction expected to be high. For a C/N ratio of 0.3, the ratio of the oxidizing valency of the oxidizer to the reducing valency of the fuel (O/R) is equal to 0.92, which is closer to unity. Compositions in the first category are fuel rich compositions and the compositions in the third category are fuel lean compositions. It is interesting to note the lower enthalpy change exhibited by the G5 and G6 batches having lower (O/R) ratios. The G3 batch with an (O/R) ratio close to 1, on the other hand exhibited the maximum enthalpy change emphasizing the effect of fuel to oxidant ratio in controlling the combustion reaction.

TG/DTA of the ash powders

The ash powders and the calcined powders derived from the different gel batches such as G1, G2, G3, G4, G5 and G6 will hereafter be designated as A1, A2, A3, A4, A5 and A6 (ash powders) and C1, C2, C3, C4, C5 and C6 (calcined powders) respectively. The TG curves of the ash powders after auto-ignition shows different decomposition behavior and clearly indicates the strong dependence of the C/N ratio (Fig. 4). The ash powders A1 and A2 decomposed in a single step whereas A3, A4, A5 and A6 decomposed in two different steps. The mass loss observed in the region 650–800 K was related to the elimination of residual carbonates and was different for different batches with varying C/N ratios. For compositions with C/N=0.08 and 0.1, a negligible mass loss was observed up to 650 K as the curve remained almost flat after 650 K indicating the absence of any carboxylate moiety in these ash powders. In the case of other compositions with higher C/N ratios two decomposition steps are evident. The first mass loss started at 300 K and ended around 650 K for the compositions A3, A4 and A6, while the same ended only at a higher temperature of 700 K for A5 ash powder. The second mass loss started at 600 K for the compositions A3, A4, A5, A6, and ended at 800 K for A3, 850 K for A5 and A6 and 950 K for A4 samples.

Table 2 Thermal characteristics of the Al_2O_3 precursor materials

Samples	Citrate/nitrate (C/N) ratio	(O/R)	Mass loss/%	Decomposition temperature T_P/K	Enthalpy $-\Delta H$/J g^{-1}
G1	0.08	3.47	87.25	498	279
G2	0.10	2.78	84.80	503	326
G3	0.30	0.92	77.49	435	436
G4	0.50	0.55	85.01	436	400
G5	0.70	0.39	88.89	449	211
G6	1.0	0.28	91.32	452	256

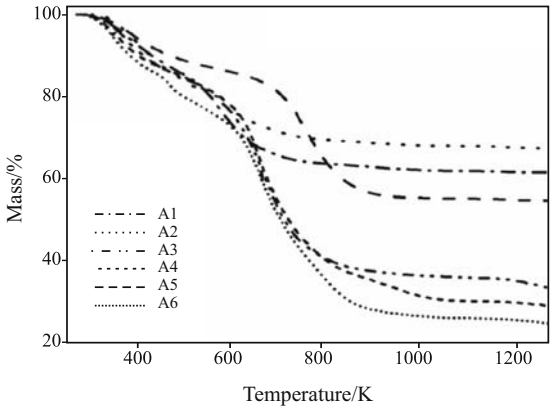

Fig. 4 TG data of different ash powders

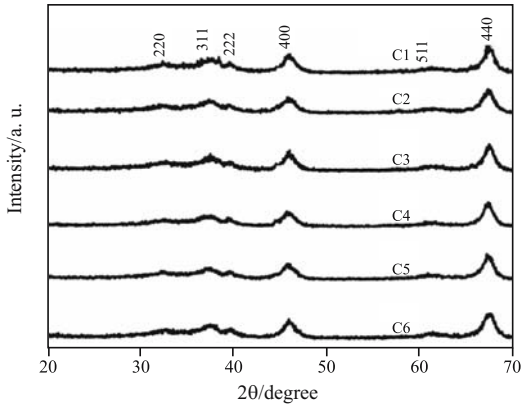

Fig. 5 XRD patterns of the 1073 K calcined precursor powder confirming the formation of γ-alumina

Comparison of the TG curves of the gels and the corresponding ash powders indicated that when the dried gel was heated slowly inside a thermal analyzer, its decomposition was complete within 850 K. On the other hand, when the gel was allowed to burn on its own on a hot plate to form the ash powder it took a slightly higher temperature (up to 973 K) for their complete removal.

X-ray diffraction analysis

The XRD analysis of the as-prepared powders of all the compositions exhibited an amorphous nature. The powders calcined at 773 K were also amorphous in nature. However, a clear transition from the amorphous state to the crystalline state could be noticed in the XRD pattern of the powders calcined at 1073 K, where γ-Al_2O_3 was the major phase (Fig. 5). The γ-phase produced as an intermediate step at 1073 K subsequently transformed to the α-phase at 1373–1473 K. The broadening of the γ-XRD peaks at 1073 K (Fig. 6) indicates the nano crystalline nature of the particles produced at this temperature. Thus, the amorphous alumina powder after calcination at

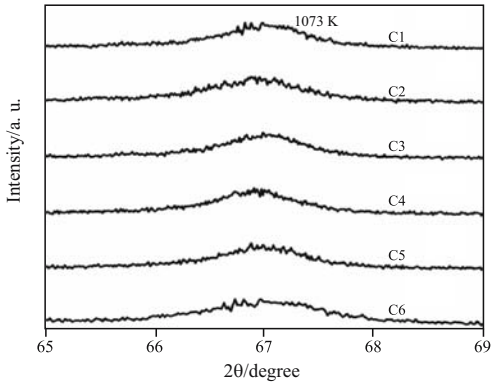

Fig. 6 Effect of C/N ratio on the line broadening of (440) reflection of the 1073 K calcined powder samples

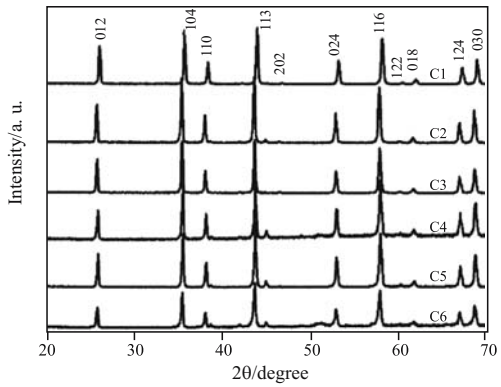

Fig. 7 XRD patterns of the1373 K calcined powders indicating the formation of α-alumina phase

1073 K transforms to γ-alumina and finally converted to α-alumina phase at 1373 K (Fig. 7). Single-phase α-alumina powder was formed after calcination at 1373 K for 6 h. Since, all the organic materials were burnt off during calcination at elevated temperatures the purity of the alumina powder was mainly controlled by the purity of the starting materials and the processing conditions.

Particle size and specific surface area

Particle size distribution of the 1073 K calcined powder is shown in Figs 8a and b respectively. The particle size and their distribution were found to depend very much on the nature of ignition of the gel, which in turn was related to the C/N ratios used. The average particle size of the powders obtained from different batches was found to depend on the fuel-nitrate ratio of the gel. From the data presented in Table 3, it is clear that the powders prepared exhibited larger particle agglomeration. Independent of the (C/N) ratio all the samples exhibited a broader size distribution (Fig. 8b). Moreover, it is also evident from Fig. 8a that a major fraction of the particles from all the batches is in a higher size range of distribution.

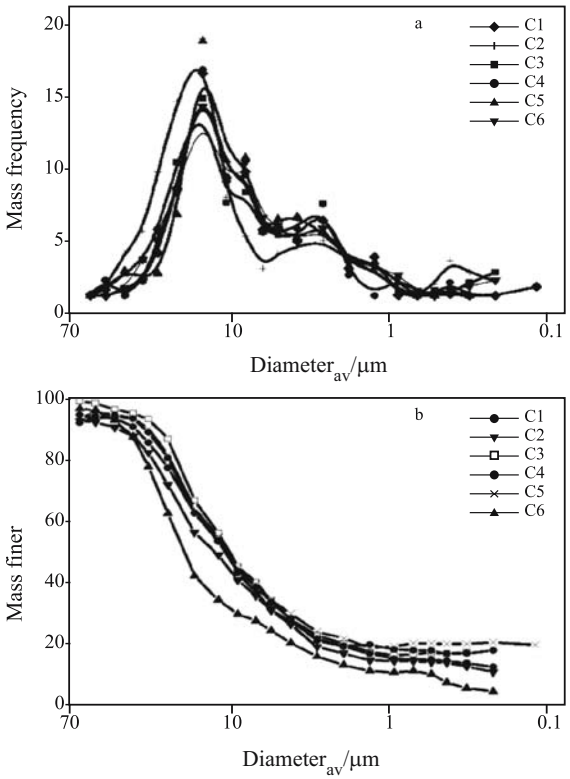

Fig. 8 Particle size distribution of the 1073 K calcined powder samples

The crystallite size of the 1073 K calcined alumina powders as calculated using Scherrer's formula is presented in Table 3. Irrespective of the preparation conditions, all the samples exhibited a crystallite size of around 4–5 nm only. A large particle size calculated from surface area compared to the crystallite size measured by XRD further illustrates the rate of agglomeration of the particles. The relative ratio between the D_{BET} and D_{XRD} designated as the extent of agglomeration is calculated and shown in Table 3. The extent of agglomeration was lowest for the powders derived from C4 batch. Neverthless, since the data were very similar (Table 3), we could not draw a definite correlation between the C/N ratio and the extent of agglomeration based on these results.

The surface area of the calcined powders at 1073 and 1373 K are given in Table 3. The surface area was higher for the 1073 K calcined powders compared to that at 1373 K. This indicates that upon calcination, due to the increased grain growth during the phase transformation from γ-Al_2O_3 to α-Al_2O_3 a substantial reduction in surface area had occurred. In contrast to the surface area of the 1073 K calcined powder, the surface area of the 1373 K calcined powders gradually decreased with increase in the C/N ratio.

Densification studies on the alumina powder compacts

The 1073 K calcined powders were cold pressed in the form of the 12 mm diameter pellets at a compaction pressure of 20 MPa using a uni-axial hydraulic press and were sintered at different temperatures. The sintered densities were determined using Archimede's principle and the corresponding (%) densification at two different temperatures is plotted in Fig. 9. The sintered density exhibited a strong relation to the fuel content in the precursor gel. Green density of the powder compacts on the other hand was more or less same irrespective of the synthetic conditions. The powder derived from G3 batch exhibited a dramatically improved densification and density more than 90% compared to other batches as evident from Fig. 9,

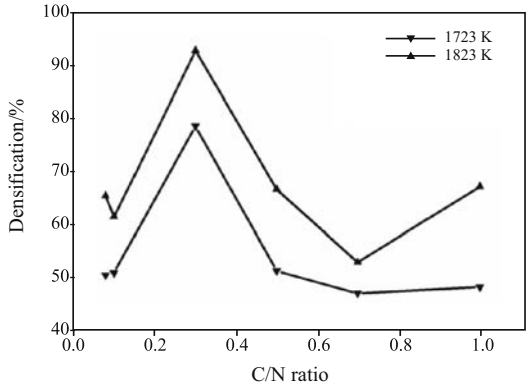

Fig. 9 Effect of C/N ratio on the densification of alumina powder compacts

Table 3 Physico-chemical characteristics of the 1073 K/6 h and 1373 K/6 h calcined powder samples

Samples	D_{XRD}/nm 1073 K/6 h	S_{BET}/m^2 g^{-1} 1073 K/6 h	D_{BET}/nm 1073 K/6 h	Extent of agglomeration D_{BET}/D_{XRD}/nm	D_{50}/μm	S_{BET}/m^2 g^{-1} 1373 K/6 h	D_{BET}/nm 1373 K/6 h
C1	4.7	45	36	7	8	25	60
C2	4.7	40	40	8	7	13	108
C3	4.7	50	32	6	6	20	72
C4	4.8	65	24	5	7	18	82
C5	4.7	45	36	7	8	36	41
C6	4.7	51	31	6	14	13	108

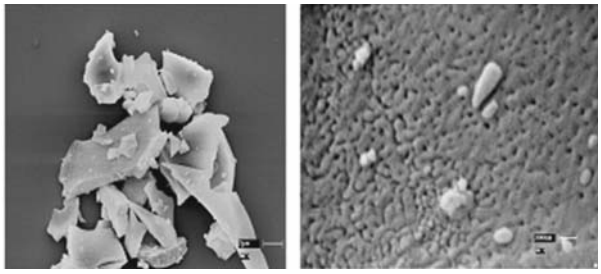

Fig.10 SEM pictures of the 1073 K calcined powder sample from G3 batch

indicating a better sinterability of the powder derived from G3 batch with an (O/R) ratio close to one. In Fig. 10, SEM picture of the 1073 K calcined G3 powder, which is used for sintering studies, is shown. The general nature of the sample is of flake type comprised of nano particles of 50–100 nm in size.

The thermal analysis results and the XRD results indicate that the probable route of α-alumina formation is from γ-alumina which has nucleated from the amorphous ash powder formed during auto-ignition. Most importantly, there was no indication of any crystallization up to 773 K and above which γ-phase has started growing. In addition, the effect of citrate to nitrate ratio (C/N) and the importance of maintaining stoichiometric ratio is also established through thermal analysis and X-ray diffraction experiments.

Conclusions

This paper reports the synthesis of nano-crystalline alumina powder by the auto-ignition of a citrate-nitrate precursor gel and the effect of variation of the citrate to nitrate (C/N) ratio on the decomposition characteristics of the corresponding gel samples. Stoichiometric and off-stoichiometric C/N ratios were selected for this purpose. It was found that the decomposition nature of the gel and the characteristics of the resultant powder could be controlled by careful control of the citrate-nitrate ratio in the gel. The best results were obtained for a C/N ratio of 0.3. A dependence of the C/N ratio on both the specific surface area and the particle size of the alumina powders calcined at 1073 and 1373 K have been noticed. The as-prepared amorphous powder yielded nano-crystalline γ-alumina at 1073 K and α-alumina at 1373 K. This auto-ignition of the citrate-nitrate gel is a very simple and convenient route to produce alumina in either the γ form or in the α-form by proper choice of the C/N ratio and the calcination temperature.

Acknowledgements

The authors thank Director, Central Glass and Ceramic Research Institute (CGCRI) for permission to publish this work. S. Banerjee is indebted to Council of Scientific and Industrial Research (CSIR) for the award of Senior Research Fellowship (SRF). Technical assistance from the X-ray division of CGCRI is acknowledged. The authors also thank all the members of the Electroceramics Division for their cooperation at every stage of this work.

References

1 B. E. Yoldas, J. Mater. Sci., 11 (1976) 465.
2 J. G. Li and X. Sun, Acta Mater., 48 (2000) 3103.
3 P. K. Sharma, V. V. Varadan and V. K. Varadan, J. Eur. Ceram. Soc., 23 (2003) 659.
4 C. S. Nordahl and G. L. Messing, J. Eur. Ceram. Soc., 22 (2002) 415.
5 L. Fu, D. L. Johnson, J. G. Zheng and V. P. Dravid, J. Am. Ceram. Soc., 86 (2003) 1635.
6 C. P. Lin, S. B.Wen and T. T. Lee, J. Am. Ceram. Soc., 85 (2002) 129.
7 R. H. G. A. Kiminami, M. R. Morelli, D. C. Folz and D. E. Clark, Am. Ceram. Soc. Bull., (2000) 63.
8 A. H. Carim, G. S. Rohrer, N. R. Dando, S. Y. Tzeng, C. L. Rohrer and A. J. Perrotta, J. Am. Ceram. Soc., 80 (1997) 2677.
9 A. Krell and H. Ma, Nanostruct. Mater., 11 (1999) 1141.
10 H. C. Park, Y. J. Park and R. Stevens, Mater. Sci. Eng. A., 367 (2004) 166.
11 X. Wang and G. Lu, Mater. Chem. Phys., 90 (2005) 225.
12 W. Kucza, J. Oblakowski, R. Gajerski, S. Labus, M. Danielewski, A. Malecki, J. Morgiel and A. Michalski, J. Therm. Anal. Cal., 88 (2007) 65.
13 B. S. Maruthiprasad, M. N. Sastri, S. Rajagopal, K. Seshan, K. R. Krishnamurthy and T. S. R. Prasada Rao, J. Therm. Anal. Cal., 34 (1988) 1023.
14 O. Mekasuwandumrong, V. Pavarajarn, M. Inoue and P. Praserthdam, Mater. Chem. Phys., 100 (2006) 445.
15 D. M. Ibrahim, T. Khalil and A. A. Mostafa, Ceram. Int., 25 (1999) 273.
16 V. Siva Kumar, G. Kelekanjeri, W. B. Carter and J. M. Hampikian, Thin Solid Films., 515 (2006) 1905.
17 S. Bhaduri, E. Zhou and S. B. Bhaduri, Nanostruct. Mater., 7 (1996) 487.
18 J. J. Kingsley and K. C. Patil, Mater. Lett., 6 (1988) 427.
19 R. N. Das, A. Bandopadhyay and S. Bose, J. Am. Ceram. Soc., 84 (2001) 2421.
20 R. L. Smith and S. V. Yanina, J. Am. Ceram. Soc., 85 (2002) 2325.
21 F. S. Shiau and T. T. Fang, Mater. Chem. Phys., 60 (1999) 91.
22 L. C. Pathak, T. B. Singh, S. Das, A. K. Verma and P. Ramachandrarao, Mater. Lett., 57 (2002) 380.
23 C. C. Chen and K. T. Huang, J. Mater. Res., 20 (2005) 424.
24 M. T. Hernandez and M. Gonzalez, J. Eur. Ceram. Soc., 22 (2002) 2861.
25 J. C. Toniolo, M. D. Lima, A. S. Takimi and C. P. Bergmann, Mater. Res. Bull., 40 (2005) 561.

26 J. Li, Y. Pan, C. Xiang, Q. Ge and J. Guo, Ceram. Inter., 32 (2006) 587.
27 J. Li, Y. Wu, Y. Pan and J. Guo, Ceram. Int., 33 (2007) 361.
28 L. Baca, J. Plewa, L. Pach and J. Opfermann, J. Therm. Anal. Cal., 66 (2001) 803.
29 M. Planda and P. Staszczuk, J. Therm. Anal. Cal., 62 (2000) 561.
30 M. Pyzalski and M. Wojcik, J. Thermal Anal., 36 (1990) 2147.
31 C. Navok, G. Pokol, V. Izvekov and T. Gal, J. Thermal Anal., 36 (1990) 1895.
32 P. S. Devi and M. S. Rao, Thermochim. Acta, 153 (1989) 181.
33 P. S. Devi and M. S. Rao, J. Thermal Anal., 48 (1997) 909.
34 L. W. Tai and P. A. Lessing, J. Mater. Res., 7 (1992) 502.
35 A. Chakraborty, P. S. Devi, S. Roy and H. S. Maiti, J. Mater. Res., 9 (1994) 986.
36 A. Chakraborty, P. S. Devi and H. S. Maiti, Mater. Lett., 20 (1994) 63.
37 A. Chakraborty, P. S. Devi and H. S. Maiti, J. Mater. Res., 10 (1995) 918.
38 S. Basu, P. S. Devi and H. S. Maiti, J. Mater. Res., 19 (2004) 3162.
39 S. Banerjee and P. S. Devi, J. Nanoparticle Res., DOI: 10.1007/s11051-006-9204-4.

DOI: 10.1007/s10973-007-8525-6